

NANOGrav Signal from double-inflection-point inflation

Tie-Jun Gao*

*School of Physics and Optoelectronic Engineering,
Xidian University, Xi'an 710071, China*

Abstract

Recently, the NANOGrav collaboration has published an analysis of its 12.5-year PTA data, which can be interpreted as a cosmological stochastic GW background. In this paper, we shall investigate the possibility to explain the NANOGrav signal by the GWs induced from inflationary models with double-inflection-point. Such double-inflection-point can be generated from polynomial potential or from the supergravity theory with a single chiral superfield. In such models, the inflection point at large scales leads to a nearly scale-invariant spectrum, which is consistent with current CMB constraints. Another inflection point leads to a large peak in the scalar power spectrum at small scales, which induce GWs at frequencies around nanohertz to explain the recent NANOGrav signal.

Keywords: inflation, gravitational waves, NANOGrav

* tjgao@xidian.edu.cn

I. INTRODUCTION

The North American Nanohertz Observatory for Gravitational Waves(NANOGrav) has recently released its 12.5-year observation of pulsar timing array(PTA) data, where strong evidence of a stochastic process, which can be explained by the stochastic GWs with a power-law spectrum $\Omega_{GW} \propto f^{5-\gamma}$ at a reference frequency of $f_{yr} \simeq 3.1 \times 10^{-8}\text{Hz}$, with the exponent $5 - \gamma \in (-1.5, 0.5)$ at 1σ confidence level[1–7].

It is well known that at first order in perturbation theory the scalar and tensor perturbations are decoupled, however, at second order the free wave equation of tensor perturbations gets a source term of scalar perturbations. Thus, when the scalar perturbations reenter the Hubble radius in the radiation-dominated(RD) era, it can leads to the production of second-order GWs [8, 9], and if the power spectrum of scalar perturbations is enhanced at small scales, the induced GWs can be sizable to be detected by experiments in near future [10–22]. The enhancement of the scalar power spectrum at small scales can be realized in the inflationary models with an inflection point [23–28]. Since the first and second order derivatives of the potential vanish near the inflection point, so the Hubble slow-roll parameter $|\eta_H| > 3$ and the ultra-slow-roll trajectory supersedes the slow-roll one, which gives rise to a large peak in the scalar power spectrum and induces GWs. The inflection point can be generated in critical Higgs inflation with the running of a large non-minimal coupling [29–31], or in the framework of string theory [32–35] etc.

In the previous models, the potential contains single inflection point, and the inflation will last about more than 30 e-folding numbers before the inflection point. Thus when the inflaton meets the inflection point, it will leads to a large peak in the power spectrum and induced GWs around millihertz, which couldn't explain the NANOGrav result around nanohertz. So in this paper we investigate the possibility to explain the NANOGrav signal by the GWs induced from inflationary models with double-inflection-point. We first consider a toy model with a polynomial potential motivated from the framework of effective field theory. We derive the primordial power spectrum of scalar perturbations, and calculate the energy spectrum of the induced GWs numerically. We find that in such a model, the inflection point at CMB scales can make the predictions consistent with the Planck 2018 data[36] and

last about 20 e-folding numbers, thus when the inflaton meets the second inflection point, it will induce GWs with the peak at frequencies around nanohertz, which can explain the recent NANOGrav signal.

Although cosmological inflation is now established by all precise observational data such as the WMAP [37] and Planck data [36], the nature of inflation is still unknown. An interesting framework for inflationary models building is to embed inflationary models into a more fundamental theory of quantum gravity, such as supergravity[38–43]. So in this paper we also consider the double-inflection-point inflationary model realized from supergravity with a single chiral superfield. Such model can both make the predictions of scalar spectral index and tensor-to-scalar ratio consistent with the current CMB constraints, and induce GWs at frequencies around nanohertz to explain the NANOGrav signal.

The paper is organized as follows. In the next section, we discuss the feasibility of explaining the results of NANOGrav experiment using a polynomial potential with double-inflection-point. In Sec.3, we setup the double-inflection-point inflationary model in the framework of supergravity, then derive the primordial power spectrum of scalar perturbations, and calculate the energy spectrum of the induced GWs numerically. The last section is devoted to summary.

II. A POLYNOMIAL POTENTIAL WITH DOUBLE-INFLECTION-POINT

In this section, we shall discuss the possibility to explain the NANOGrav signal using inflationary potential with double-inflection-point, and such inflection points can be generated from a polynomial potential.

A. The Model

Motivated from the framework of an effective field theory with a cutoff scale Λ , a polynomial potential is generally given by[44–49]

$$V_{\text{eff}}(\phi) = \sum_{n=0} \frac{b_n}{n!} \left(\frac{\phi}{\Lambda}\right)^n. \quad (1)$$

In order to build a model with double-inflection-point, there must at least four free parameters. If we ignore the constant term and first order term to make the potential and its first-order derivative vanish at the origin, the effective potential is truncated to the sixth order as

$$V_{\text{eff}}(\phi) = V_0 \left[\frac{c_2}{2!} \left(\frac{\phi}{\Lambda} \right)^2 + \frac{c_3}{3!} \left(\frac{\phi}{\Lambda} \right)^3 + \frac{c_4}{4!} \left(\frac{\phi}{\Lambda} \right)^4 + \frac{c_5}{5!} \left(\frac{\phi}{\Lambda} \right)^5 + \frac{1}{6!} \left(\frac{\phi}{\Lambda} \right)^6 \right], \quad (2)$$

where the overall factor V_0 can be constrained by the amplitude of scalar perturbations A_s , and c_{2-5} are four free parameters.

The inflection point is such point that both the first and second derivatives of V vanish. So for convenience of discussion, we assume that the potential have two inflection points at $\phi_i (i = 1, 2)$ respectively, where $V'(\phi_i) = 0$ and $V''(\phi_i) = 0$. More generally, in order to study the slight deviations from a perfect inflection point, we introduce two more free parameters α_i and set $V'(\phi_i) = \alpha_i$ and $V''(\phi_i) = 0$. Then the parameters $c_{2\sim 5}$ in Eq.(2) can be expressed as functions of ϕ_i and α_i . In some choices of parameter space, one can get a potential with double-inflection-point, which both consistent with the CMB constraints and induce a second-order GWs at frequencies around nanohertz.

For instance, we take the following parameter set

$$\begin{aligned} V_0 &= 1.553 \times 10^{-10}, \quad \Lambda = 1, \\ \phi_1 &= 0.91, \quad \alpha_1 = -5.4164 \times 10^{-6}, \\ \phi_2 &= 2.1, \quad \alpha_2 = 3 \times 10^{-6}, \end{aligned} \quad (3)$$

and equivalently, the parameters in Eq.(2) are

$$c_2 = 0.0304286, \quad c_3 = -0.191766, \quad c_4 = 0.644212, \quad c_5 = -1.20411. \quad (4)$$

Then we show the corresponding potential in Fig.1.

We can see that the potential contains double-inflection-point. The inflation starts near the first inflection point at CMB scales and leads to a nearly scale-invariant spectrum, then rolls down the plateau-like region slowly. Whenever the inflaton meets a cliff, it speeds up quickly, until it reaches the next inflection point plateau and slow down again. Such point leads to a ultra-slow-roll phase last about 35 e-folding numbers, which generates a large

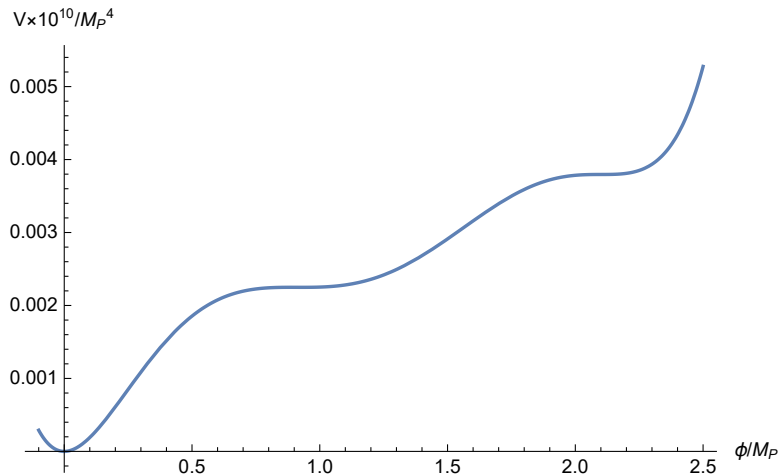


FIG. 1: Scalar potential for the polynomial model with parameter set (3).

peak in the power spectrum, and induce a second-order GW spectrum which can explain the NANOGrav signal.

B. Inflation dynamics

In the FRW homogeneous background, the Friedmann equation and the scalar field equation are

$$H^2 = \frac{1}{3M_P^2} \left(\frac{1}{2} \dot{\phi}^2 + V(\phi) \right), \quad (5)$$

$$\ddot{\phi} + 3H\dot{\phi} + V'(\phi) = 0, \quad (6)$$

with dots represent derivatives with respect to cosmic time and primes denote derivatives with respect to the field ϕ . And the e-folding numbers from an initial time t_i is defined as

$$N_e(t) = \int_{t_i}^t H(t) dt. \quad (7)$$

In the framework slow-roll inflation, the slow-roll parameters are defined as

$$\begin{aligned} \epsilon &= \frac{M_P^2}{2} \left(\frac{V'}{V} \right)^2, \\ \eta &= M_P^2 \left(\frac{V''}{V} \right). \end{aligned} \quad (8)$$

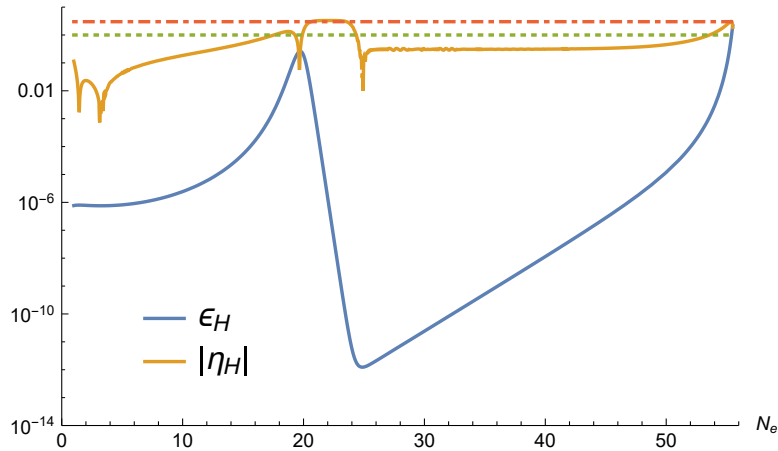


FIG. 2: The Hubble slow-roll parameters ϵ_H and η_H as functions of the e-folding number N_e for the polynomial model with parameter set (3).

However, in the inflationary models with inflection points, the potential is extremely flat near the inflection point, and the ultra-slow-roll trajectory supersedes the slow-roll one [50–53]. Thus one must use the slow-roll parameters defined by the Hubble parameters [54–56],

$$\begin{aligned}\epsilon_H &= -\frac{\dot{H}}{H^2}, \\ \eta_H &= -\frac{\ddot{H}}{2H\dot{H}} = \epsilon_H - \frac{1}{2} \frac{d \ln \epsilon_H}{dN_e},\end{aligned}\quad (9)$$

In Fig.2, we show the Hubble slow-roll parameters ϵ_H and η_H as functions of the e-folding numbers N_e for the polynomial model with parameter set (3).

We can see that near the second inflection point the Hubble slow-roll parameter $|\eta_H| > 3$, so the slow-roll approximation fails and the inflation becomes ultra-slow-roll, which gives rise to a large valley on the curve of ϵ_H lasting more than 30 e-folding numbers.

It has been pointed out in several references that near the inflection point, the calculation of the scalar spectrum using the approximate expression $\mathcal{P}_{\mathcal{R}} \simeq \frac{1}{8\pi^2 M_P^2} \frac{H^2}{\epsilon_H}$ will underestimate the power spectrum [26]. Thus in order to compute the power spectrum more reliably, one must numerically solve the Mukhanov-Sasaki (MS) equation of mode function,

$$\frac{d^2 u_k}{d\tau^2} + \left(k^2 - \frac{1}{z} \frac{d^2 z}{d\tau^2} \right) u_k = 0, \quad (10)$$

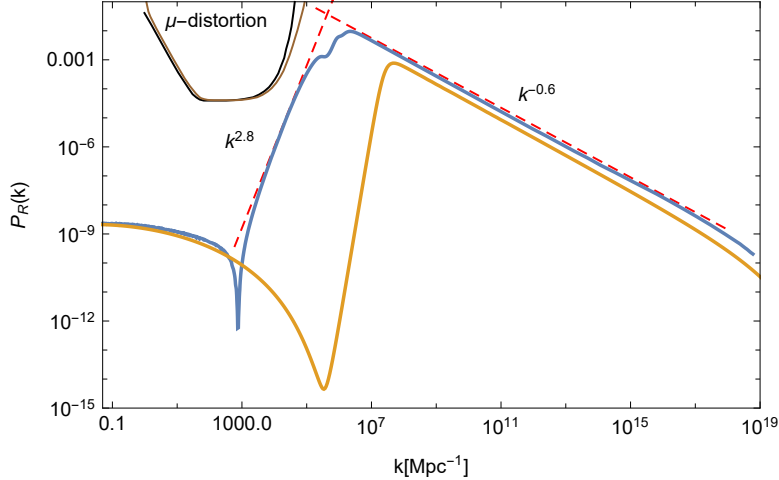


FIG. 3: Primordial power spectrum of scalar perturbations predicted by the polynomial model for parameter set (3). And the upper bound from μ -distortion for a delta function power spectrum(Black line) and for the steepest growth k^4 power spectrum(Brown line)[58].

with $z \equiv \frac{a}{\mathcal{H}} \frac{d\phi}{d\tau}$. And the initial condition is taken to be the Bunch-Davies type[57],

$$u_k \rightarrow \frac{e^{-ik\tau}}{\sqrt{2k}}, \quad \text{as } \frac{k}{aH} \rightarrow \infty. \quad (11)$$

where τ denotes conformal time. Then the power spectrum can be calculated by

$$\mathcal{P}_{\mathcal{R}} = \frac{k^3}{2\pi^2} \left| \frac{u_k}{z} \right|_{k \ll \mathcal{H}}^2. \quad (12)$$

Our numerical results of scalar power spectrum for the polynomial model with parameter set (3) are shown in Fig.3. Where the blue line is the numerical result of the MS equation while the orange line is the approximate result, which underestimate the power spectrum. And the constraints to the primordial power spectrum from μ -distortion are also show there.

We can see that the scalar power spectrum has a large peak at small scales with a height of about seven orders of magnitude higher than the spectrum at CMB scales, which will leads to the production of non-negligible second-order GWs.

It is interesting to note that the power spectrum can be parameterized as the broken power form $\mathcal{P}_{\mathcal{R}} \sim k^n$. we find that in our models which is $k^{2.8}$ before the peak and $k^{-0.6}$

after the peak (the red dashed line of Fig.4). In Ref.[58], the authors pointed out that in canonical single field inflation, the steepest growth index of the power spectrum before the peak is k^4 , and in our models the result are slower than k^4 .

At the leading order, the scalar spectral index as well as the tensor-to-scalar ratio can be expressed using ϵ_H and η_H as

$$\begin{aligned} n_s &= 1 - 4\epsilon_H + 2\eta_H, \\ r &= 16\epsilon_H. \end{aligned} \tag{13}$$

For the polynomial model with parameter set (4), the numerical results are $n_s = 0.9672$, $r = 0.0000122$, the amplitude of the primordial curvature perturbations A_s and the e-folding numbers during inflation N_e are $\ln(10^{10}A_s) = 3.0443$, $N_e = 55.4$. The results are in agreement with the current CMB constraints $n_s = 0.9649 \pm 0.0042$, $r < 0.064$ and $\ln(10^{10}A_s) = 3.044 \pm 0.014$ from Planck 2018 [36].

C. Gravitational waves induced by scalar perturbations

It is well-known that at second order, tensor perturbations are coupled to scalar perturbations, so the second-order GWs can be induced from the amplified scalar perturbations, and can be detected by GW experiments. In the follows, we first present the formalism of the induced GWs, for more details in Ref.[59–64], then give numerical results by using the power spectrum obtained in the province subsection.

In the conformal Newtonian gauge, the perturbed metric can be expressed as

$$ds^2 = -a^2(1 + 2\Psi)d\eta^2 + a^2 \left[(1 - 2\Psi)\delta_{ij} + \frac{1}{2}h_{ij} \right] dx^i dx^j, \tag{14}$$

where Ψ is the scalar perturbations, and the Fourier modes of tensor perturbations h_{ij} are defined as

$$h_{ij}(\eta, \mathbf{x}) = \int \frac{d^3\mathbf{k}}{(2\pi)^{3/2}} e^{i\mathbf{k}\cdot\mathbf{x}} \left[h_{\mathbf{k}}^+(\eta) e_{ij}^+(\mathbf{k}) + h_{\mathbf{k}}^\times(\eta) e_{ij}^\times(\mathbf{k}) \right], \tag{15}$$

with the polarization tensors $e_{ij}^+(\mathbf{k})$ and $e_{ij}^\times(\mathbf{k})$ satisfy $\sum_{i,j} e_{ij}^\alpha(\mathbf{k}) e_{ij}^\beta(-\mathbf{k}) = \delta^{\alpha\beta}$. In the following, we shall omit the polarization index for simplicity.

In the Fourier space, the equation of motion of tensor modes is obtained from the Einstein equation to the second order

$$h_{\mathbf{k}}''(\eta) + 2\mathcal{H}h_{\mathbf{k}}'(\eta) + k^2h_{\mathbf{k}}(\eta) = S_{\mathbf{k}}(\eta), \quad (16)$$

with $S_{\mathbf{k}}(\eta)$ denotes the Fourier transformation of the source term, which is given by

$$S_{\mathbf{k}}(\eta) = 4 \int \frac{d^3p}{(2\pi)^{3/2}} e_{ij}(\mathbf{k}) p_i p_j \left(2\Psi_{\mathbf{p}}\Psi_{\mathbf{k}-\mathbf{p}} + \frac{4}{3(1+w)\mathcal{H}^2} (\Psi'_{\mathbf{p}} + \mathcal{H}\Psi_{\mathbf{p}}) (\Psi'_{\mathbf{k}-\mathbf{p}} + \mathcal{H}\Psi_{\mathbf{k}-\mathbf{p}}) \right), \quad (17)$$

where the equation of state is taken $\omega = 1/3$ if the peak mode enters the horizon in the RD era.

For the modes well inside the horizon, the energy spectrum of the GWs within the logarithmic interval of the wave numbers can be expressed in terms of the power spectrum

$$\Omega_{\text{GW}}(\eta, k) = \frac{1}{24} \left(\frac{k}{\mathcal{H}} \right)^2 \overline{\mathcal{P}_h(\eta, k)}, \quad (18)$$

where the overline denotes the oscillation average and the two polarization modes of GWs have been summed up.

Using the Green's function method, and considering $\mathcal{H} = 1/\eta$ in the RD era, the energy spectrum can be obtained as

$$\begin{aligned} \Omega_{\text{GW}}(\eta, k) &= \frac{1}{12} \int_0^\infty dv \int_{|1-v|}^{1+v} du \left(\frac{4v^2 - (1+v^2 - u^2)^2}{4uv} \right)^2 \mathcal{P}_{\mathcal{R}}(ku) \mathcal{P}_{\mathcal{R}}(kv) \\ &\quad \left(\frac{3}{4u^3v^3} \right)^2 (u^2 + v^2 - 3)^2 \\ &\quad \left\{ \left[-4uv + (u^2 + v^2 - 3) \ln \left| \frac{3 - (u+v)^2}{3 - (u-v)^2} \right| \right]^2 + \left[\pi (u^2 + v^2 - 3) \Theta(u+v - \sqrt{3}) \right]^2 \right\} \end{aligned} \quad (19)$$

where $u \equiv |\mathbf{k} - \mathbf{p}|/k$, $v \equiv |\mathbf{p}|/k$ and $x \equiv k\eta$ are three dimensionless variables [13].

The GW energy spectrum at the present time $\Omega_{\text{GW},0}$ is related to the one produced in the RD era as[61]

$$\Omega_{\text{GW},0} = 0.83 \left(\frac{g_{*,0}}{g_{*,p}} \right)^{-1/3} \Omega_{r,0} \Omega_{\text{GW}}, \quad (20)$$

with $\Omega_{r,0} \simeq 9.1 \times 10^{-5}$ is the current density fraction of radiation, $g_{*,0}$ and $g_{*,p}$ are the effective degrees of freedom for energy density at the present time and at the time when the peak mode crosses the horizon, respectively.

Combine the numerical result of scalar power spectrum $\mathcal{P}_{\mathcal{R}}$ obtained in the previous subsection, we numerically calculate the energy spectrum of induced GWs and show it in Fig.5, with the horizontal axis is the present value of the frequency

$$f \approx 0.03\text{Hz} \frac{k}{2 \times 10^7 \text{pc}^{-1}}. \quad (21)$$

The sensitivity curves of several planned GW detectors are also shown there [31, 65–69].

Recently, the NANOGrav collaboration has published an analysis of 12.5-year of PTA, which can be fitted by the stochastic GWs with a power-law spectrum around $f_{yr} \simeq 3.1 \times 10^{-8}\text{Hz}$,

$$\Omega_{GW}(f) = \frac{2\pi^2 f_{yr}^2}{3H_0^2} A_{GWB}^2 \left(\frac{f}{f_{yr}} \right)^{5-\gamma}, \quad (22)$$

where $H_0 \equiv 100h$ km/s/Mpc and the exponent $5 - \gamma \in (-1.5, 0.5)$ at 1σ confidence level[1–7]. The observed GWs for $5 - \gamma = 0$ with 2σ uncertainty on A_{GWB} are also show in Fig.4. We can see that the frequencies of the energy spectrum of induced GWs cover from nanohertz to millihertz, and the maximum is at the frequency $f = 3.97 \times 10^{-9}\text{Hz}$, which is within the frequency range of SKA and EPTA. The induced GW spectrum at frequencies around nanohertz lies in the 2σ region of the NANOGrav constraints, so it can explain the NANOGrav signals. And around millihertz, the energy spectrum curves lies above the expected sensitivity curves ASTROD-GW, so such kind of GWs can be detected by the GW detectors in near future.

III. DOUBLE-INFLECTION-POINT FROM SUPERGRAVITY WITH A SINGLE CHIRAL SUPERFIELD

In this section, we shall setup the inflationary model with double-inflection-point in supergravity and calculate the primordial power spectrum of scalar perturbations and the energy spectrum of induced GWs numerically.

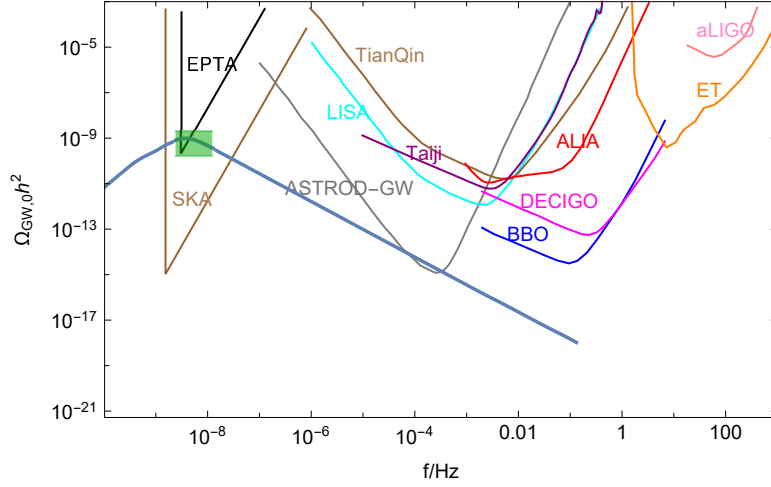


FIG. 4: Energy spectrum of the induced GWs at the present time predicted by the polynomial model for parameter set (3). The curves in the upper part are the expected sensitivity curves of the European Pulsar Timing Array (EPTA), Square Kilometer Array (SKA), Laser Interferometer Space Antenna (LISA), Taiji, TianQin, Astrodynamical Space Test of Relativity using Optical-GW detector (ASTROD-GW), Advanced Laser Interferometer Antenna (ALIA), Big Bang Observer (BBO), Deci-hertz Interferometer GW Observatory (DECIGO), Einstein Telescope (ET), Advanced LIGO (aLIGO), respectively. These sensitivity curves are taken from Ref. [31, 65–69] The green region show the 2σ confidence level of the NANOGrav results with the tilt of $5 - \gamma = 0$ [1].

A. The Model

Consider a shift-symmetric Kähler potential of the form[70]

$$K = ic(\Phi - \bar{\Phi}) - \frac{1}{2}(\Phi - \bar{\Phi})^2 - \frac{\zeta}{4}(\Phi - \bar{\Phi})^4, \quad (23)$$

with c and ζ are two real constants. The real component ϕ of the chiral superfield $\Phi = (\phi + i\chi)/\sqrt{2}$ is taken to be the inflaton and the quartic term $\frac{\zeta}{4}(\Phi - \bar{\Phi})^4$ serves to stabilize the field ϕ during inflation at $\langle \chi \rangle \simeq 0$ by making ζ sufficient large.

In some inflationary models favoured by the CMB data, the scalar potential can be generated by a superpotential which can be expanded as[70, 71],

$$W = \sum_{n \geq 0} a_n e^{-b_n \Phi}, \quad (24)$$

with a_n and b_n are constants. So in order to generate a potential with double-inflection-point, we consider an exponential superpotential of the form

$$W = a_0(1 + a_1e^{-b_1\Phi} + a_2e^{-b_2\Phi} + a_3e^{-b_3\Phi}). \quad (25)$$

Such a kind of superpotentials with exponential functions with two terms have been studied in the so-called racetrack model[71–73] and in other models[70]. If we require the SUSY preservation in vacuum with a vanishing cosmological constant(The issue of SUSY breaking in vacuum has been discussed in Ref.[42]), the F-term should be vanished $D_\Phi W = 0$, and $V = 0$ at $\Phi = 0$, which requires the constraint

$$W = \partial_\Phi W = 0. \quad (26)$$

Then we can eliminate two of the parameters a_1 and a_2 by solving the constraint above

$$a_1 \rightarrow \frac{b_2 + a_3b_2 - a_3b_3}{b_1 - b_2}, a_2 \rightarrow \frac{-b_1 - a_3b_1 + a_3b_3}{b_1 - b_2}. \quad (27)$$

Substituting the superpotential (23) and Kähler potential (25) into

$$V = e^{K/M_P^2} \left[D_{\Phi_i} W (K^{-1})^{ij*} D_{\Phi_j^*} W^* - 3M_P^{-2} |W|^2 \right], \quad (28)$$

one can get the scalar potential $V(\phi)$. Where

$$D_\Phi W = \partial_\Phi W + M_P^{-2} (\partial_\Phi K) W, \quad (29)$$

and $(K^{-1})^{ij*}$ is the inverse of the Kähler metric

$$K^{ij*} = \frac{\partial^2 K}{\partial \Phi_i \partial \Phi_j^*}. \quad (30)$$

In some choices of parameter space, such superpotential and Kähler potential can generate a potential with double-inflection-point, which both predict an approximate scale invariant spectrum at CMB scales and induce a second-order GW spectrum which can explain the NANOGrav signal. For instance, we take the following parameter set

$$\begin{aligned} a_0 &= 4.35 \times 10^{-6}, & a_3 &= 7 \times 10^{-8}, & c &= 2.8, \\ b_1 &= 3.05, & b_2 &= 6.3868164, & b_3 &= -4.4, \end{aligned} \quad (31)$$

and plot the corresponding scalar potential in Fig.5.

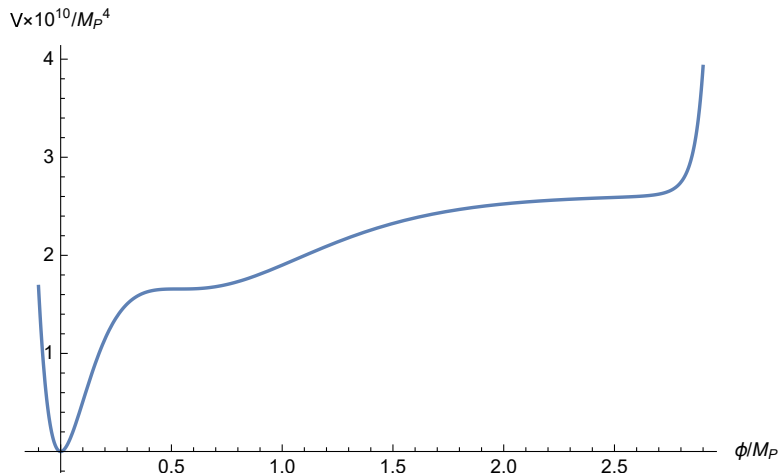


FIG. 5: Scalar potential for the supergravity model with parameter set (31).

We can see that the potential contains two inflection points, one of the inflection points at high scales can make the prediction of scalar spectral index and tensor-to-scalar ratio consistent with the current CMB data, and the other one at small scales can lead to a phase of ultra-slow-roll which induces a second-order GW spectrum with a peak around nanohertz to explain the NANOGrav signal. The numerical results are shown in the following subsections.

Moreover, after inflation, one can obtain small SUSY breaking and a tiny cosmological constant by introducing a nilpotent superfield [74, 75].

B. Numerical Results

Using the parameter set (31), we calculate the Hubble slow-roll parameters ϵ_H and η_H numerically, and show them as functions of the e -folding numbers N_e in Fig.6. Similar as in the polynomial model, the Hubble slow-roll parameter $|\eta_H| > 3$ near the second inflection points, so the ultra-slow-roll process replaces the slow-roll one, and gives rise to a large valley on the curve of ϵ_H lasting about 35 e -folding numbers. Our numerical results of the scalar spectral index as well as the tensor-to-scalar ratio are $n_s = 0.963323$, $r = 0.00834467$, the amplitude of the primordial curvature perturbations A_s is $\ln(10^{10}A_s) = 3.04127$, and the e -folding numbers during inflation is $N_e = 53.18$. Which are all in agreement with the Planck 2018

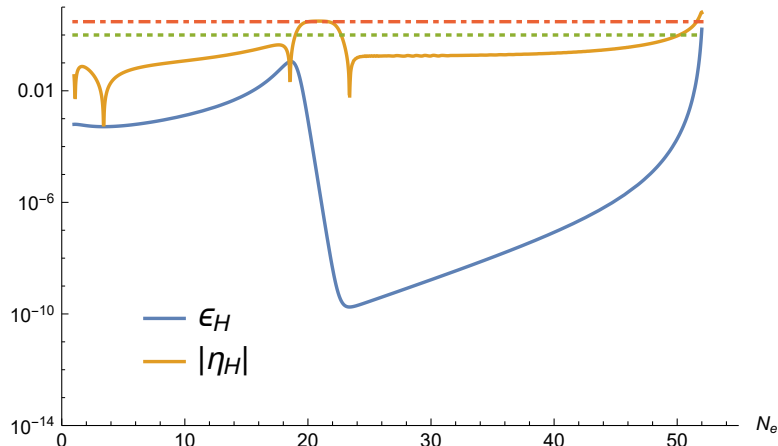


FIG. 6: The Hubble slow-roll parameters ϵ_H and η_H as functions of the e-folding number N_e for the supergravity model with parameter set (31).

observations at CMB scales[36].

By solving the MS equation of mode function numerically, we get the scalar power spectrum for the supergravity model with parameter set (31) and show it in Fig.7(the blue line), while the approximate result are also show there (the orange line), which underestimate the power spectrum. We can see that height of the peak at small scales is about seven orders of magnitude more than the spectrum at CMB scales, which will lead to the production of non-negligible second-order GWs. And in this model, the growth index of the power spectrum is k^3 before the peak, which is slower than k^4 , and $k^{-0.37}$ after the peak(the red dashed line of Fig.7).

The numerically result of the energy spectrum of induced GWs using the scalar power spectrum $\mathcal{P}_{\mathcal{R}}$ obtained above are shown in Fig.8, where the sensitivity curves of several planned GW detectors are also shown there [31, 65–69]. And the green region is the 2σ confidence level of the NANOGrav results with the tilt of $5 - \gamma = 0$ [1]. In this model, the maximum of the frequencies of induced GWs at the frequency around nanohertz, which is within the frequency range of SKA and EPTA, and the curves lies in the 2σ region of the NANOGrav constraints, so it can explain the NANOGrav signal. At frequencies around millihertz the energy spectrum curves lies above the expected sensitivity curves of ASTROD-GW, and also above BBO, thus it can also be detected by the detectors.

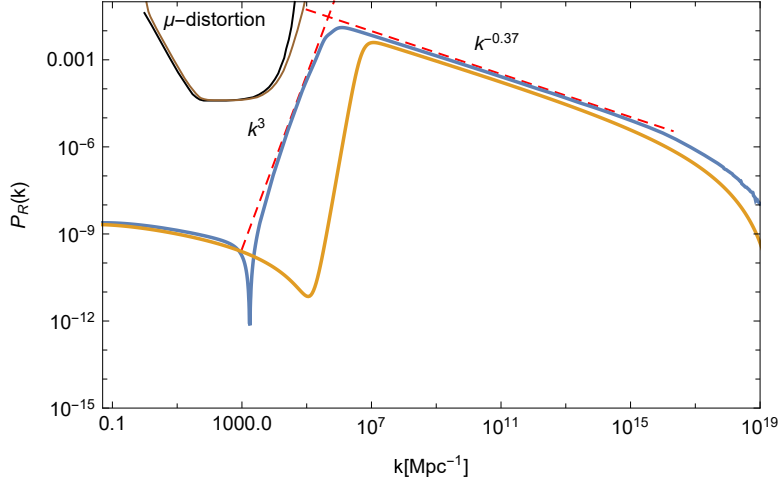


FIG. 7: Primordial power spectrum of scalar perturbations predicted by the supergravity model for parameter set (31). And the upper bound from μ -distortion for a delta function power spectrum(Black line) and for the steepest growth k^4 power spectrum(Brown line)[58].

IV. SUMMARY

In this paper, we investigate the possibility to explain the recent NANOGrav signal by the inflationary models with double-inflection-point. We find that such potential can be realized by the polynomial potential from effective field theory with a cut off scale or realized in the framework of supergravity with a single chiral superfield. For some choices of parameter sets, the inflection point at large scales make the prediction of scalar spectral index and tensor-to-scalar ratio consistent with the current CMB constraints, and the other inflection point generates a large peak in the power spectrum at small scales to induce GWs. We calculate the energy spectrum of GWs numerically and shown that the the peak is at frequencies around nanohertz, which is within the frequency range of SKA and EPTA, and lies in the 2σ uncertainty of NANOGrav, so it can explain the NANOGrav signal. In addition, around millihertz, the energy spectrum curves lies above the expected sensitivity curves of ASTROD-GW for both models, and above BBO for the supergravity model, so such kind of GWs can be detected by the GW detectors in near future. Moreover, the large peak in the scalar spectrum can leads to the production of primordial balck holes

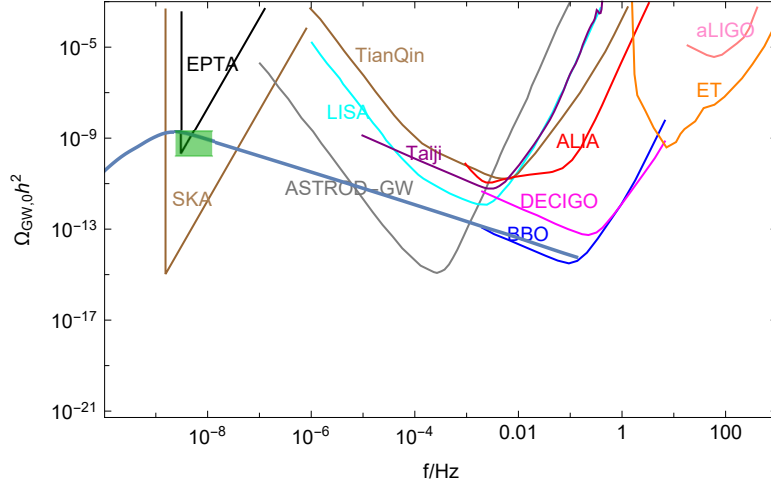


FIG. 8: Energy spectrum of the induced GWs at the present time predicted by the supergravity model for parameter set (27). The expected sensitivity curves in the upper part are the same as in Fig.4. And the green region also show the 2σ confidence level of the NANOGrav results with the tilt of $5 - \gamma = 0$ [1].

(PBHs)[76–81], thus we also calculate the abundance of PBHs produced in the two models using the Press-Schechter approach of gravitational collapse, and found that the peak mass of PBHs is around $10^{-16} \sim 10^{-15} M_{\odot}$ and the fraction in dark matter is very small, which didn't overproduce.

ACKNOWLEDGMENTS

This work was supported by “the National Natural Science Foundation of China” (NNSFC) with Grant No. 11705133.

-
- [1] Z. Arzoumanian *et al.* [NANOGrav], *Astrophys. J. Lett.* **905** (2020) no.2, L34 [arXiv:2009.04496 [astro-ph.HE]].
 - [2] V. Vaskonen and H. Veermäe, *Phys. Rev. Lett.* **126** (2021) no.5, 051303 [arXiv:2009.07832 [astro-ph.CO]].
 - [3] K. Kohri and T. Terada, *Phys. Lett. B* **813** (2021), 136040 [arXiv:2009.11853 [astro-ph.CO]].

- [4] V. De Luca, G. Franciolini and A. Riotto, *Phys. Rev. Lett.* **126** (2021) no.4, 041303 [arXiv:2009.08268 [astro-ph.CO]].
- [5] M. Kawasaki and H. Nakatsuka, [arXiv:2101.11244 [astro-ph.CO]].
- [6] S. Vagnozzi, *Mon. Not. Roy. Astron. Soc.* **502** (2021) no.1, L11-L15 doi:10.1093/mnrasl/slaa203 [arXiv:2009.13432 [astro-ph.CO]].
- [7] G. Domènech and S. Pi, [arXiv:2010.03976 [astro-ph.CO]].
- [8] S. Matarrese, S. Mollerach and M. Bruni, *Phys. Rev. D* **58**, 043504 (1998) [astro-ph/9707278].
- [9] V. Acquaviva, N. Bartolo, S. Matarrese and A. Riotto, *Nucl. Phys. B* **667**, 119 (2003) [astro-ph/0209156].
- [10] H. Assadullahi and D. Wands, *Phys. Rev. D* **79**, 083511 (2009) [arXiv:0901.0989 [astro-ph.CO]].
- [11] L. Alabidi, K. Kohri, M. Sasaki and Y. Sendouda, *JCAP* **1209**, 017 (2012) [arXiv:1203.4663 [astro-ph.CO]].
- [12] L. Alabidi, K. Kohri, M. Sasaki and Y. Sendouda, *JCAP* **1305**, 033 (2013) [arXiv:1303.4519 [astro-ph.CO]].
- [13] K. Kohri and T. Terada, *Phys. Rev. D* **97**, no. 12, 123532 (2018) [arXiv:1804.08577 [gr-qc]].
- [14] R. G. Cai, S. Pi and M. Sasaki, *Phys. Rev. Lett.* **122**, no. 20, 201101 (2019) [arXiv:1810.11000 [astro-ph.CO]].
- [15] K. Inomata and T. Nakama, *Phys. Rev. D* **99**, no. 4, 043511 (2019) [arXiv:1812.00674 [astro-ph.CO]].
- [16] R. G. Cai, S. Pi, S. J. Wang and X. Y. Yang, arXiv:1901.10152 [astro-ph.CO].
- [17] J. Fumagalli, S. Renaux-Petel and L. T. Witkowski, [arXiv:2012.02761 [astro-ph.CO]].
- [18] J. Garcia-Bellido, M. Peloso and C. Unal, *JCAP* **09** (2017), 013 [arXiv:1707.02441 [astro-ph.CO]].
- [19] C. Unal, *Phys. Rev. D* **99** (2019) no.4, 041301 [arXiv:1811.09151 [astro-ph.CO]].
- [20] G. Domènech, *Int. J. Mod. Phys. D* **29** (2020) no.03, 2050028 [arXiv:1912.05583 [gr-qc]].
- [21] G. Domènech and M. Sasaki, *Phys. Rev. D* **103** (2021) no.6, 063531 [arXiv:2012.14016 [gr-qc]].
- [22] G. Domènech, [arXiv:2109.01398 [gr-qc]].

- [23] J. Garcia-Bellido and E. Ruiz Morales, Phys. Dark Univ. **18**, 47 (2017) [arXiv:1702.03901 [astro-ph.CO]].
- [24] C. Germani and T. Prokopec, Phys. Dark Univ. **18**, 6-10 (2017) [arXiv:1706.04226 [astro-ph.CO]].
- [25] H. Di and Y. Gong, JCAP **1807**, no. 07, 007 (2018) [arXiv:1707.09578 [astro-ph.CO]].
- [26] Guillermo Ballesteros, Marco Taoso. Phys.Rev. D97 (2018) no.2, 023501. [arXiv:1709.05565]
- [27] I. Dalianis, A. Kehagias and G. Tringas, JCAP **1901**, 037 (2019) [arXiv:1805.09483 [astro-ph.CO]].
- [28] T. J. Gao and X. Y. Yang, Int. J. Mod. Phys. A **34** (2019) no.32, 1950213
- [29] J. M. Ezquiaga, J. Garcia-Bellido and E. Ruiz Morales, Phys. Lett. B **776**, 345-349 (2018) [arXiv:1705.04861 [astro-ph.CO]].
- [30] F. Bezrukov, M. Pauly and J. Rubio, JCAP **02**, 040 (2018) [arXiv:1706.05007 [hep-ph]].
- [31] M. Drees and Y. Xu, arXiv:1905.13581 [hep-ph].
- [32] O. Özsoy, S. Parameswaran, G. Tasinato and I. Zavala, JCAP **07**, 005 (2018) [arXiv:1803.07626 [hep-th]].
- [33] T. J. Gao and X. Y. Yang, Int. J. Mod. Phys. A **34**, no.32, 1950213 (2019)
- [34] M. Cicoli, V. A. Diaz and F. G. Pedro, JCAP **06**, 034 (2018) doi:10.1088/1475-7516/2018/06/034 [arXiv:1803.02837 [hep-th]].
- [35] J. Liu, Z. K. Guo and R. G. Cai, Phys. Rev. D **101**, no.8, 083535 (2020) [arXiv:2003.02075 [astro-ph.CO]].
- [36] Y. Akrami *et al.* [Planck Collaboration], arXiv:1807.06211 [astro-ph.CO].
- [37] G. Hinshaw et al. [WMAP Collaboration], Astrophys. J. Suppl. **208** (2013) 19; [arXiv:1212.5226]
- [38] D. Z. Freedman, P. van Nieuwenhuizen and S. Ferrara, Phys. Rev. D **13** (1976) 3214.
- [39] S. Deser and B. Zumino, Phys. Lett. B **62** (1976) 335.
- [40] J. Wess and J. Bagger, Supersymmetry and Supergravity (Princeton University Press: Princeton, New Jersey, 1992), 2nd Edition.
- [41] Supergravity based inflation models: a review. [arXiv:1101.2488]
- [42] T. J. Gao and Z. K. Guo, Phys. Rev. D **91**, 123502 (2015) [arXiv:1503.05643 [hep-th]].

- [43] T. J. Gao, W. T. Xu and X. Y. Yang, *Mod. Phys. Lett. A* **32** (2017) no.2, 1750072 [arXiv:1606.05951 [hep-ph]].
- [44] N. Bhaumik and R. K. Jain, *JCAP* **01**, 037 (2020) [arXiv:1907.04125 [astro-ph.CO]].
- [45] K. Enqvist and A. Mazumdar, *Phys. Rept.* **380**, 99-234 (2003) [arXiv:hep-ph/0209244 [hep-ph]].
- [46] C. P. Burgess, H. M. Lee and M. Trott, *JHEP* **09**, 103 (2009) [arXiv:0902.4465 [hep-ph]].
- [47] F. Marchesano, G. Shiu and A. M. Uranga, *JHEP* **09**, 184 (2014) [arXiv:1404.3040 [hep-th]].
- [48] M. P. Hertzberg, M. Yamada *Phys. Rev. D* **97**, 083509 (2018) [arXiv:1712.09750 [astro-ph.CO]]
- [49] G. Ballesteros, J. Rey, M. Taoso and A. Urbano *JCAP* **07** (2020) 025 [arXiv:2001.08220 [astro-ph.CO]]
- [50] C. Germani and T. Prokopec, *Phys. Dark Univ.* **18**, 6 (2017) [arXiv:1706.04226 [astro-ph.CO]].
- [51] K. Dimopoulos, *Phys. Lett. B* **775**, 262 (2017) [arXiv:1707.05644 [hep-ph]].
- [52] J. M. Ezquiaga and J. Garca-Bellido, *JCAP* **1808** (2018) 018, [arXiv:1805.06731 [astro-ph]].
- [53] D. Cruces, C. Germani and T. Prokopec, *JCAP* **1903** (2019) no.03, 048 , [arXiv:1807.09057 [gr-qc]].
- [54] D. J. Schwarz, C. A. Terrero-Escalante and A. A. Garcia, *Phys. Lett. B* **517**, 243 (2001) [astro-ph/0106020].
- [55] S. M. Leach, A. R. Liddle, J. Martin and D. J. Schwarz, *Phys. Rev. D* **66**, 023515 (2002) [astro-ph/0202094].
- [56] D. J. Schwarz and C. A. Terrero-Escalante, *JCAP* **0408**, 003 (2004) [hep-ph/0403129].
- [57] T. S. Bunch and P. C. W. Davies, *Proc. Roy. Soc. Lond. A* **360** (1978), 117-134
- [58] C. T. Byrnes, P. S. Cole and S. P. Patil, *JCAP* **06** (2019), 028 doi:10.1088/1475-7516/2019/06/028 [arXiv:1811.11158 [astro-ph.CO]].
- [59] D. Baumann, P. J. Steinhardt, K. Takahashi and K. Ichiki, *Phys. Rev. D* **76**, 084019 (2007) [hep-th/0703290].
- [60] K. N. Ananda, C. Clarkson and D. Wands, *Phys. Rev. D* **75**, 123518 (2007) [gr-qc/0612013].
- [61] K. Ando, K. Inomata, M. Kawasaki, K. Mukaida and T. T. Yanagida, *Phys. Rev. D* **97** (2018) no.12, 123512 [arXiv:1711.08956 [astro-ph.CO]].

- [62] H. Kodama and M. Sasaki, Prog. Theor. Phys. Suppl. **78**, 1 (1984).
- [63] V. F. Mukhanov, H. A. Feldman and R. H. Brandenberger, Phys. Rept. **215**, 203 (1992).
- [64] J. R. Espinosa, D. Racco, and A. Riotto JCAP 09 (2018) 012 [arXiv:1804.07732 [hep-ph]].
- [65] H. Audley et al. [arxiv:1702.00786 [astro-ph.IM]].
- [66] Z. K. Guo, R. G. Cai and Y. Z. Zhang, arXiv:1807.09495 [gr-qc].
- [67] C. J. Moore, R. H. Cole and C. P. L. Berry, Class. Quant. Grav. **32** (2015) no.1, 015014, [arXiv:1408.0740 [gr-qc]].
- [68] J. Luo et al. [TianQin Collaboration], Class. Quant. Grav. **33** (2016) no.3, 035010, [arXiv:1512.02076 [astro-ph.IM]].
- [69] K. Kuroda, W. T. Ni and W. P. Pan, Int. J. Mod. Phys. D **24** (2015) no.14, 1530031, [arXiv:1511.00231 [gr-qc]].
- [70] Sergei V. Ketov, Takahiro Terada. On SUSY Restoration in Single-Superfield Inflationary Models of Supergravity. Eur.Phys.J. C **76** (2016) no.8, 438. [arXiv:1606.02817]
- [71] J.J. Blanco-Pillado, C.P. Burgess, James M. Cline et.al. Racetrack inflation. JHEP 0411 (2004) 063.
- [72] C. Escoda, M. Gomez-Reino, and F. Quevedo, Saltatory de Sitter string vacua, JHEP 11 (2003) 065, [arXiv:hep-th/0307160]
- [73] N.V. Krasnikov, On supersymmetry breaking in superstring theories, Phys. Lett. B **193** (1987) 37
- [74] S. Ferrara, R. Kallosh, and A. Linde, Cosmology with Nilpotent Superfields, JHEP 10 (2014) 143, [arXiv:1408.4096].
- [75] R. Kallosh and A. Linde, Inflation and Uplifting with Nilpotent Superfields, JCAP 1501 (2015) 025, [arXiv:1408.5950].
- [76] J. Yokoyama, Astron. Astrophys. **318**, 673 (1997) [astro-ph/9509027].
- [77] J. Garcia-Bellido, A. D. Linde and D. Wands, Phys. Rev. D **54**, 6040 (1996) [astro-ph/9605094].
- [78] S. Clesse and J. Garcia-Bellido, Phys. Rev. D **92**, no. 2, 023524 (2015) [arXiv:1501.07565 [astro-ph.CO]].

- [79] J. Garcia-Bellido, M. Peloso and C. Unal, *JCAP* **1612**, no. 12, 031 (2016) [arXiv:1610.03763 [astro-ph.CO]].
- [80] S. L. Cheng, W. Lee and K. W. Ng, *JHEP* **1702**, 008 (2017) doi:10.1007/JHEP02(2017)008 [arXiv:1606.00206 [astro-ph.CO]].
- [81] C. Fu, P. Wu and H. Yu, arXiv:1907.05042 [astro-ph.CO].
- [82] G. Ballesteros and M. Taoso, Primordial black hole dark matter from single field inflation, *Phys. Rev. D* **97**, 023501 (2018).
- [83] B. J. Carr, The primordial black hole mass spectrum, *Astrophys. J.* **201**, 1 (1975).
- [84] I. Musco and J. C. Miller, Primordial black hole formation in the early universe: Critical behaviour and self-similarity, *Classical Quantum Gravity* **30**, 145009 (2013).
- [85] T. Harada, C.-M. Yoo, and K. Kohri, Threshold of primordial black hole formation, *Phys. Rev. D* **88**, 084051 (2013); Erratum, *Phys. Rev. D* **89**, 029903(E) (2014).